Antifungal Potential of *Diaporthe* sp. Endophytes from Antillean Avocado Against *Fusarium* spp.: From Organic Extracts to *In Silico* Chitin Synthase Inhibition

Angie T. Robayo-Medina *, Katheryn Michell Camargo-Jimenez, Felipe Victoria-Muñoz, Wilman Delgado-Avila, Luis Enrique Cuca, Mónica Ávila-Murillo *

Posted Date: 10 December 2025

doi: 10.20944/preprints202512.0969.v1

Keywords: *Persea americana* var. *americana*; *Diaporthe* sp.; *Fusarium solani*; *Fusarium equiseti*; Chitin Synthase; molecular docking

 doi:10.20944/preprints202512.0969.v1

Article

Antifungal Potential of *Diaporthe* sp. Endophytes from Antillean Avocado Against *Fusarium* spp.: From Organic Extracts to *In Silico* Chitin Synthase Inhibition

Angie T. Robayo-Medina [1,*], Katheryn-Michell Camargo-Jimenez [1], Felipe Victoria-Muñoz [2], Wilman Delgado-Avila [3], Luis Enrique Cuca [3] and Mónica Ávila-Murillo [3,*]

[1] Universidad Nacional de Colombia, Sede Bogotá, Facultad de Ciencias, Departamento de Química. Grupo de Investigación Estudio Químico de Productos Naturales Vegetales Bioactivos- QUIPRONAB. Bogotá D.C., Colombia

[2] Fundación Universitaria Salesiana, Facultad de Ciencias Exactas y Naturales. Grupo de Investigación FarmaBioTech. Bogotá D.C., Colombia

[3] Universidad Nacional de Colombia, Sede Bogotá, Facultad de Ciencias, Departamento de Química. Grupo de Investigación QUIPRONAB. Bogotá D.C., Colombia

* Correspondence: atrobayom@unal.edu.co (A.T.R.-M.); mcavilam@unal.edu.co (M.Á.-M.)

Abstract

Fungal endophytes have emerged as a promising source of bioactive compounds with potent antifungal properties for plant disease management. This study aimed to isolate and characterize fungal endophytes from Antillean avocado (*Persea americana* var. *americana*) trees in the Colombian Caribbean, capable of producing bio-fungicide metabolites against *Fusarium solani* and *Fusarium equiseti*. For this, dual-culture assays, liquid-state fermentation of endophytic isolates, and metabolite extractions were conducted. From 88 isolates recovered from leaves and roots, those classified within the *Diaporthe* genus exhibited the most significant antifungal activity. Their organic extracts displayed median inhibitory concentrations (IC_{50}) approaching 200 µg/mL. To investigate the mechanism of action, *in silico* studies targeting Chitin Synthase (CS) were performed, including homology models of the pathogens' CS generated using Robetta, followed by molecular docking with Vina, and interaction fingerprint similarity analysis of 15 antifungal metabolites produced by *Diaporthe* species using PROLIF. A consensus scoring strategy identified diaporxanthone A (**12**) and diaporxanthone B (**13**) as the most promising candidates, achieving scores up to 0.73 against *F. equiseti*, comparable to the control Nikkomycin Z (0.82). These results suggest that Antillean avocado endophytes produce bioactive metabolites that may inhibit fungal cell wall synthesis, offering a sustainable alternative for disease management.

Keywords: *Persea americana* var. *americana*; *Diaporthe* sp.; *Fusarium solani*; *Fusarium equiseti*; Chitin Synthase; molecular docking

1. Introduction

Species of the *Fusarium* genus rank among the most detrimental phytopathogens globally, causing toxin contamination as well as severe diseases and economic losses across a broad spectrum of crops, including cereals, vegetables, and tropical fruits. [1,2] These pathogens induce chlorosis and cotyledon necrosis, water-soaked lesions on the crown and lower stem, pre-emergence and post-emergence growth retardation, brown to black wilt in the lower main root and lateral roots, vascular damage and, in some cases, produce mycotoxins harmful to human and animal health. [3,4]

 doi:10.20944/preprints202512.0969.v1

Current strategies for controlling *Fusarium* infections encompass the use of resistant crop varieties, implementation of best agricultural practices, and application of synthetic fungicides like phosphine, formaldehyde, carbendazim, thiophanate-methyl or propiconazole + prochloraz, among others. [5,6] However, chemical interventions raise critical concerns regarding environmental sustainability, potential toxicity, and the accumulation of harmful residues in food products. [7] In response to these challenges, plant-microbiome interactions, particularly those involving fungal endophytes, have emerged as a promising avenue for sustainable disease management, due to their ability to enhance plant resilience against both biotic and abiotic stressors. [8–10]

Notably, the selection of host plants plays a key role in the successful isolation of endophytes, with highest bioactive potential often found in plants from unique ecosystems like tropical forests, endemic species with unusual longevity, or those that have adapted to extreme environmental conditions. [11,12] That is the case of Antillean avocados (*Persea americana* var. *americana*) growth in the Montes de María region (Colombian Caribbean). These plants have been propagated by seed over five decades leading to their classification as endemic varieties well adapted to the region's distinct climatic and geographic conditions (0-1000 m.a.s.l. and 18-27°C). [13,14] The endemic ecotypes—Cebo, Leche, and Manteca— are distinguished based on fruit characteristics, including pulp texture and fat content. However, their cultivation has been severely affected by the Avocado Wilt Complex (AWC), a group of phytopathogens including *Fusarium, Verticillium*, and *Phytophthora*, which aggressively compromise the root systems of most avocado trees. [15,16] Remarkably, the survival of some avocado plants suggests the presence of intrinsic defense mechanisms, potentially mediated by a diverse and functionally significant endophytic community. In this context, the present study aims to investigate the microbiota associated with Antillean avocado trees in Montes de María and to evaluate their potential as antifungal metabolites producers, with inhibitory activity against *F. solani* and *F. equiseti.*

In the same way, understanding the mechanisms of action of antifungal compounds is fundamental for advancing plant disease management and addressing the growing challenge of fungal resistance. Antifungal compounds target essential structures and metabolic processes in phytopathogenic fungi through multiple mechanisms of action like intracellular reactive oxygen species accumulation, cell membrane disruption, lipid peroxidation, mitochondrial dysfunction [17,18], inhibition of cell wall biosynthesis [19,20], etc. Particularly, the unique composition of the fungal cell wall—dominated by polysaccharides such as glucans and chitins, along with glycoproteins—distinguishes it fundamentally from human cellular structures. [21] Consequently, Chitin Synthase (CS), the enzyme responsible for chitin polymerization, has emerged as a strategic molecular target for the development of selective antifungal agents. [22,23] Despite its clinical and agricultural relevance, structural data for CS in specific phytopathogens such as *Fusarium solani* and *Fusarium equiseti* remain limited, often hindering the rational elucidation of inhibition mechanisms. To address this gap and investigate the molecular basis of the antifungal activity observed in this study, an *in silico* approach was integrated. We performed homology modeling to generate 3D structures of the CS enzymes for both pathogens, followed by molecular docking and interaction fingerprint (PLIF) analyses. This computational strategy was employed to evaluate whether bioactive metabolites, previously isolated from endophytic *Diaporthe* species, could act as potential inhibitors of this critical enzymatic target.

2. Materials and Methods

2.1. Collection of Plant Material

Leaves and secondary roots from the Cebo, Manteca, and Leche ecotypes of avocado (*Persea americana* var. *americana*) cultivated in the Caribbean region of Colombia (09°34′42″N 75°16′15″W), were collected in 2017. The collection of plant material and the study of the isolated fungi were covered by Permission No. 121 of January 22, 2016 (Amendment No. 21), under the Access to Genetic Resources and Derivative Products Agreement No. RGE 46 (Article 6 - Law 1955 of 2019), granted by

 doi:10.20944/preprints202512.0969.v1

Ministerio de Ambiente y Desarrollo Sostenible de Colombia. Fungal isolates were placed in the QUIPRONAB strain collection, located at the Chemistry Department of Universidad Nacional de Colombia, Sede Bogotá.

2.2. Avocado Phytopathogens Isolation

Fusarium pathogens were isolated from secondary roots of trees exhibiting symptoms of AWC. Plant material was surface sterilized following established protocols [24], and fungal isolates were identified through a combination of morphological and molecular characterization [25].

Two *Fusarium* isolates were selected based on an *in vivo* pathogenicity test. Avocado seedlings, germinated from seeds and cultivated under controlled glasshouse conditions (~18-20 °C day, ~12-15 °C night) for four months, reached 40-50 cm and developed at least four true leaves [26]. Each treatment included ten plants. Conidial suspensions (1×10^7 CFU/mL) were prepared from 14-day-old cultures grown on potato dextrose agar (PDA), and roots were immersed for 2 min prior to transplanting into sterile soil. An additional 1 mL of inoculum was applied near to the root zone. Sterile distilled water served as a negative control. Plants were irrigated weekly for six weeks, and disease severity was evaluated using a 0-3 scale: 0 (no lesion), 1 (chlorosis/slight withering), 2 (severe withering/defoliation), and 3 (plant mortality). The disease index (DI) was calculated using DI = 100 * [(a.X0) + (b.X1) + (c.X2) + (d.X3)] / (N*3), where a-d represents the number of plants at each infection level, and N is the total plants per treatment. Following the experiment, seedlings were uprooted, and the causal agents were re-isolated via root surface sterilization and subsequent culture on PDA.

2.3. Fungal Endophytes Isolation

Healthy leaves and secondary roots were collected from three Antillean avocado ecotypes -Cebo, Leche, and Manteca- that had survived adverse phytosanitary conditions in the Colombian Caribbean region. Plant material was surface sterilized following the previously described protocol. The samples were excised into 5 mm^2 segments [27] and plated onto different solid culture media, including V8 juice agar, malt extract agar, yeast glucose extract agar, and potato dextrose agar, all supplemented with chloramphenicol (400 ppm). Following the incubation period, individual fungal morphotypes were subcultured onto PDA to obtain pure isolates. To establish a well-characterized fungal collection and ensure culture purity, axenic cultures were obtained [28]. Endophytic fungal strains were subsequently preserved under cryogenic storage conditions [29] for further study.

2.4. Inhibitory Activity of Fungal Endophytes and Their Organic Extracts

Dual-culture assays were conducted on PDA plates (ø=90 mm) by placing 5 mm agar plugs of the entophytic isolate and the phytopathogen (*F. solani* or *F. equiseti*) 50 mm apart. Cultures were incubated at 28°c for 14 days and radial fungal growth was measured daily. Control plates consisting of the pathogen grow under identical conditions without endophyte interaction, were included for comparison [30]. The experiment was performed in triplicate, and only endophytes exhibiting significant inhibitory effects on pathogen growth were selected for subsequent organic extraction.

Selected endophytic isolates were cultured in 250 mL Erlenmeyer flasks containing 100 mL of 2% yeast extract broth and incubated at 28°C with constant agitation (150 rpm) for 14 days. Biotechnological products were extracted via three consecutive ultrasound-assisted extractions using 300 mL of ethyl acetate (EtOAc) per flask. The organic phase was subsequently filtered, separated, and concentrated under reduced pressure to obtain crude extracts (Liu & Liu, 2018).

Fungal extracts were tested for antifungal activity using agar dilution method in 12-well plates. A stock solution (50 mg/mL) was prepared in ethanol, from which 40 µl was combined with 10 µl of MTT (2 mg/mL) and 1950 µL of PDA, resulting in a final concentration of 1 mg/mL per well. Pathogens were inoculated using a sterile toothpick from a seven-day PDA culture and incubated at 28°C for 72 h. Growth inhibition (% MGI) was quantified using ImageJ™ and compared to untreated controls [31]. Extracts exhibiting mycelial growth inhibition (% MGI) ≥ 50% at 1000 µg/mL were

 doi:10.20944/preprints202512.0969.v1

selected for further dose-response analysis to determine IC_{50} values, employing agar dilution with concentrations between 25-3000 µg/mL. All experiments were conducted in triplicate, and IC_{50} values were calculated using GraphPad Prism software.

2.5. Morphological and Molecular Characterizations of Endophytes

Fungal endophytes exhibiting ≥50 % MGI against *Fusarium spp.* were identified through a combination of morphological and molecular analyses. Molecular identification was conducted via DNA sequence analysis of the internal transcribed spacer (ITS-1) region of ribosomal DNA, following established protocols comparisons for the internal transcribed spacer ITS-1 of the ribosomal DNA [32]. The resulting sequences were queried against GenBank using the Basic Local Alignment Search Tool (BLAST) hosted at NCBI (https://blast.ncbi.nlm.nih.gov/Blast.cgi) to identify the closest taxonomic matches [33]. All ITS-rDNA sequences were submitted to GenBank to obtain accession numbers (Table S1).

2.6. Homology Modeling and Structural Selection

The amino acid sequences of Chitin Synthase (CS) for *F. solani* and *F. equiseti* were retrieved from the UniProtKB database. [34] To identify a suitable structural template, a sequence alignment was performed using BLASTp against the Protein Data Bank (PDB) to find a crystallographic structure with high identity and query coverage. Three independent automated prediction servers were employed to generate the 3D structural models: Robetta[35], AlphaFold[36], and I-TASSER [37]. To select the most reliable structure among the generated predictions, the models were structurally superimposed onto the identified template. The final selection was determined by calculating the Root Mean Square Deviation (RMSD) of the backbone atoms relative to the template; the model exhibiting the lowest RMSD value was chosen.

2.7. Molecular Docking and Interaction Analysis

The molecular docking simulations were performed using AutoDock Vina to predict the binding affinity and orientation of the isolated metabolites within the catalytic site of CS. [38] The selected 3D models of *F. solani* and *F. equiseti* CS were prepared by adjusting the protonation states at pH 7.4 were assigned using PDB2PQR, and partial charges were added. [39] The 3D structures of the 15 fungal metabolites were generated and energy-minimized using RDKit (MMFF94 force field). [40] Gasteiger partial charges were assigned, and rotatable bonds were defined before conversion to PDBQT format using OpenBabel of all structures. [41]

The search space was defined centered on the coordinates of the reference inhibitor Nikkomycin Z (derived from the template PDB: 7WJO) and creating a cubic grid box of 8Å in each dimension to cover the active site pocket. [42] Docking runs were executed with an exhaustiveness parameter of 16. To validate the protocol, a re-docking assay was performed using the co-crystallized ligand, calculating the Root Mean Square Deviation (RMSD) between the predicted and experimental poses using spyrmsd. [43] The resulting protein-ligand complexes were analyzed to identify key molecular contacts. Interaction fingerprints (IFP) were generated using ProLIF to map hydrogen bonds, hydrophobic contacts, and pi-stacking interactions. [44] To rank the compounds, a similarity analysis was conducted by calculating the Cosine coefficient between the interaction fingerprint of each metabolite and that of the reference inhibitor (Nikkomycin Z).

To identify the most promising candidates, a consensus scoring function (consensus score) was established by integrating the binding affinity and the interaction similarity. Since the Vina score and the PROLIF similarity possess different units and scales, both variables were normalized using the Min-Max scaling method. The consensus score for each molecule was calculated as the arithmetic mean of these normalized values.

 doi:10.20944/preprints202512.0969.v1

3. Results and Discussion

3.1. Avocado Phytopathogens Isolation

Six fungal strains were isolated from the secondary roots of Antillean avocado trees exhibiting symptoms of root rot. These isolates were subjected to morphological and molecular characterization. DNA sequencing was performed to facilitate taxonomic identification (Table 1).

Table 1. Molecular characterization and GenBank accession numbers for isolates from secondary roots of Antillean avocado trees with disease symptoms.

Fungal isolate	Accession number	Closest related species	Similarity (%)
UN02	PP052962	OQ673588.1 *Epicoccum sp.*	100.00
UN23	PP052963	MG980304.1 *Colletotrichum sp.*	100.00
UN29	OQ271226.1	MN989030.1 *Fusarium solani*	100.00
UN31	PP052964	NR_130690.1 *Fusarium sp.*	100.00
UN36	PP052965	LC406903.1 *Colletotrichum sp.*	99.65
UN37	OQ344629.1	OP006756.1 *Fusarium equiseti*	100.00

After pathogenicity assay on avocado seedlings, two *Fusarium* strains could induce disease symptoms. *F. solani* and *F. equiseti* exhibited a 100% disease incidence, with disease severity indices of 77% and 80%, respectively, six weeks post-inoculation. Koch's postulates were confirmed through the successful re-isolation of the pathogens following surface disinfection of infected seedling roots and subsequent culture on PDA. Morphological identification was confirmed based on macroscopic and microscopic characteristics of the re-isolated strains.

These findings are consistent with previous reports on the phytopathogenic potential of *Fusarium* species. Indeed, *Fusarium spp.* are among the most prevalent pathogens affecting avocado crops globally, with *F. solani*, *F. equiseti*, and *F. oxysporum* recognized as the most economically significant. Typical disease symptoms include chlorosis, necrosis, water-soaked lesions, growth retardation, and root wilt [45]. In addition, previous studies have reported the disease incidence of *Fusarium* species in avocado seedlings. For instance, a study conducted in Michoacán, Mexico, on *Persea americana* var. *drymifolia* identified *F. oxysporum* and *F. solani* isolates as pathogenic, with 63% causing wilting and 16% inducing necrosis [46]. Similarly, in Kenya, *F. solani*, *F. oxysporum*, and *F. equiseti* were associated with stem-end rot in Hass avocados, with disease severity ranging from 19.2% to 60.8% [47]. All about, and our findings further establish *Fusarium* as a major pathogen in avocado cultivation.

Although *Phytophthora cinnamomi* is a primary causal agent of root rot in Colombian avocado orchards [48,49], it was not recovered in this study. Previous research has reported the presence of oomycetes like *P. cinnamomi*, *P. citricola*, and *P. heveae*, as well as fungal pathogens including *Lasiodiplodia theobromae*, *Pythium spp.*, *Fusarium spp.*, and *Verticillium spp.*, in Hass avocado plantations in Antioquia, with disease incidence ranging from 10% to 65% [50]. Additionally, *Phytophthora heveae*, *Calonectria spp.*, and *Fusarium spp*. have been identified in avocado nurseries in Valle del Cauca [51]. In *Persea americana* var. *americana* (Antillean avocado), *P. cinnamomi* has been identified as the primary causal agent of wilt, with an incidence exceeding 40% in 2009 [16]. Moreover, recent studies suggest that *Colletotrichum spp.* contribute to abnormal seedling development and formation of necrotic acervuli in nurseries settings. Additionally, other pathogenic organisms including *P. cinnamomi*, *Sclerotium rolfsii*, and *Nectria spp.*, have been implicated in symptoms such as wilting, necrosis, and terminal stem/root rot [52].

 doi:10.20944/preprints202512.0969.v1

3.2. Avocado Fungal Endophytes Isolation

Following surface disinfection and incubation of plant material, a total of 88 strains were selected as different morphotypes based on their growth on PDA. Of these, 19 endophytic fungi were isolated from avocado roots and 69 were recovered from leaves. Most isolates were obtained from Cebo and Manteca avocado ecotypes, whereas the Leche ecotype exhibited the lowest percentage of fungal endophytes (17%). This reduced endophyte diversity in Leche ecotype may be related to observations reported by local avocado growers, who indicate that this ecotype has been the most susceptible to phytopathogenic infections. Consequently, the Leche ecotype has become increasingly rare in the Montes de María region (Oral communication, Asociación de Productores de Aguacate Tecnificado de los Montes de María, Asproatemom, 2017).

Avocado plants in the Colombian Caribbean, particularly those in Montes de María, serve as reservoirs of microbiological diversity due to their longevity and endemic characteristics. Three key traits distinguish these ecotypes: (1) seed-based propagation, (2) adaptation to tropical environments, and (3) resilience to adverse phytosanitary conditions. These factors contribute to the establishment of endophytic communities with significant bioactive potential. Vertical transmission through seeds facilitates the persistence of endophytes across generations, thereby enhancing host survival and conferring resistance against pathogens. Moreover, the high plant diversity in tropical regions has been correlated with abundant and chemically diverse endophytes [53]. Additionally, endophytes modulate host phenotypes through mutualistic interactions, enhancing stress tolerance by producing antimicrobial metabolites and activating systemic defense mechanisms against pathogens [54].

The inhibitory activity of 88 fungal endophytes was assessed using dual culture assays. After 14 days of incubation, avocado-associated endophytes exhibited four distinct antagonistic interactions: 1). Competition for space and nutrients, promoting high colonization density (Figure 1A); 2). Mycoparasitism, characterized by endophytic overgrowth on the pathogen's mycelium and the formation of appressoria on hyphae (Figure 1B); 3). Fumigant activity via volatile organic compounds (VOCs), validated through separate inoculation and confrontation assays (Figure 1C) [55]; and 4). Antibiosis, wherein extracellular enzymes, volatiles, and antibiotics inhibited pathogen growth (Figure 1D). In this study, antibiosis was the primary selection criterion for identifying isolates with antifungal potential, with 35 strains exhibiting inhibitory effects against *F. solani* and 29 against *F. equiseti.*

Figure 1. Biocontrol effects of fungal endophytes isolated from Antillean avocado leaves and roots, against *Fusarium* phytopathogens after 14 days of incubation. (left: endophyte; right: pathogen). Growth control of *F. solani* (Figure 1.E), and *F. equiseti* (Figure 1.F).

The production of secondary metabolites is typically more pronounced during the late exponential or stationary growth phases, requiring adjustments in harvest time to optimize yield.

 doi:10.20944/preprints202512.0969.v1

Notably, most filamentous fungi undergo a 7-day culture for metabolite extraction [56]. Given this, the 35 endophytes isolated from Antillean avocado leaves and roots that exhibited antifungal activity against *Fusarium spp.* in dual culture assays were incubated for 14 days prior to organic extraction using ethyl acetate (EtOAc). In an agar dilution assay, eight EtOAc extracts demonstrated >50% inhibition of at least one *Fusarium* pathogen at 1000 µg/mL. However, extracts UN76, UN104, and UN106, derived from Leche and Cebo ecotypes, unexpectedly promoted *F. solani* growth (Table 2, Figure 2).

Table 2. % MGI of endophytic extract at 1000 µg/mL against *Fusarium* pathogens. Data shows media value ± standard deviation. N/E: Not evaluated (Endophytes didn´t show growth inhibition zones of pathogens in dual cultures).

Endophytic EtOAc extract N.	% MGI		Endophytic EtOAc extract N.	% MGI	
	F. solani	*F. equiseti*		*F. solani*	*F. equiseti*
UN22	**66,2 ± 0,5^{h,A}**	**68,6 ± 2,0^{a,A}**	UN100	12,8 ± 2,5^{e}	27,1 ± 0,6^{h}
UN39	**57,7 ± 1,2^{i}**	**70,9 ± 3,2^{a}**	UN102	7,3 ± 1,1^{a,d}	15,5 ± 2,1^{j}
UN51	50,2 ± 0,3	**57,1 ± 3,3^{b}**	UN103	6,2 ± 0,9a,d	36,7 ± 1,6^{f}
UN68	5,6 ± 2,9a	30,3 ± 2,1g	UN104	-6,8 ± 1,0c	N/E
UN70	0,9 ± 2,2b,B	3,0 ± 1,7B	UN105	35,1 ± 1,0	39,1 ± 2,5d,e
UN71	3,8 ± 2,5a,b	8,9 ± 1,5k	UN106	-3,6 ± 1,0c	17,7 ± 1,1i,j
UN76	-5,1 ± 1,4c	21,3 ± 3,4i	UN107	24,9 ± 1,3g	43,8 ± 2,5e
UN77	41,2 ± 1,2k	46,2 ± 2,0d	UN112	11,5 ± 2,3e	18,7 ± 0,7i,j
UN79	2,4 ± 2,7a,b	13,5 ± 3,1j	UN113	13,2 ± 1,2e	24,1 ± 1,2h
UN80	18,9 ± 3,2f,C	20,8 ± 2,7i,C	UN115	8,0 ± 2,2a,d,e	21,7 ± 2,6i
UN82	24,5 ± 3,1g	N/E	UN122	25,6 ± 1,8g	29,0 ± 1,6g,h
UN86	4,3 ± 2,4a,D	6,7 ± 2,2k,D	UN123	14,0 ± 2,2e	25,3 ± 1,7h
UN87	18,3 ± 1,8f	25,9 ± 3,1h	UN301	9,7 ± 1,3d,e	21,0 ± 0,8i
UN92	**70,1 ± 1,6^{j}**	**57,1 ± 2,0^{b}**	UN302	22,8 ± 0,7g	28,0 ± 2,7g
UN93	**63,1 ± 0,7^{h}**	19,9 ± 1,67	UN310	**60,8 ± 1,6^{h,i,E}**	**61,3 ± 1,0^{b,c,E}**
UN94	7,4 ± 1,5a,d	N/E	UN314	14,3 ± 1,6e,f,F	16,0 ± 2,6j,F
UN95	**60,7 ± 0,9^{h,i}**	51,1 ± 3,7e	UN318	18,0 ± 1,6f	21,6 ± 1,8i
UN99	**59,6 ± 2,9^{h,i}**	**53,4 ± 0,5^{e}**	---	---	---

Values followed by the same lowercase letters in the columns of %ICM for each pathogen at 1000 µg/mL do not show significant differences according to Tukey's test ($p > 0.05$). Similarly, means followed by the same uppercase letters in the rows are not significantly different in a one-way ANOVA analysis ($p > 0.05$). Bold type: most promising antifungal extracts.

The antifungal activity of the extracts evaluated in this study was comparable to that of other extracts described in the literature as promising inhibitors of *Fusarium* species. For example, the crude extract of the endophyte *Fusarium proliferatum*, obtained with EtOAc, showed 75.51% inhibition of *F. oxysporum* at a concentration of 1000 µg/mL [57]. Similarly, the EtOAc extract of the endophyte *Chaetomium globosum* exhibited mycelial growth inhibition percentages of 59.06%, 64.90%, and 59.41% against *F. graminearum, F. oxysporum*, and *F. moniliforme*, respectively [58].

 doi:10.20944/preprints202512.0969.v1

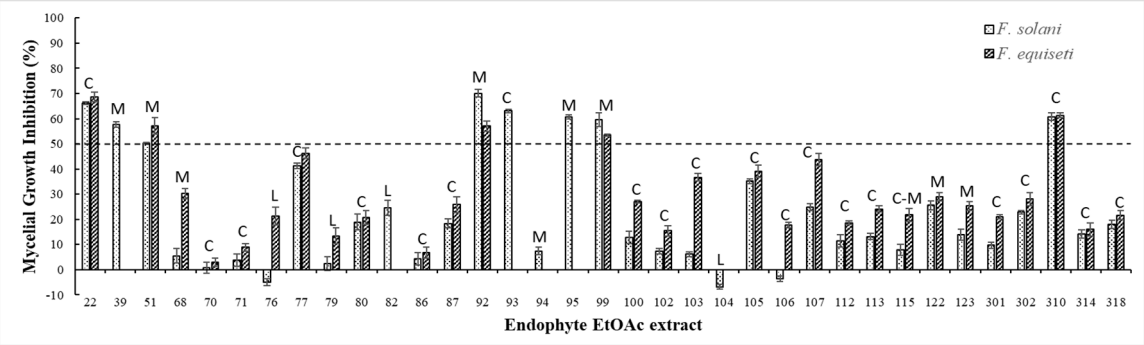

Figure 2. Origin of Antillean avocado endophytes that showed inhibitory activity on *F. solani* and *F. equiseti* growth in dual cultures. The graphic highlights those which their EtOAc extracts exhibited % MGI of at least one pathogen over 50% in the agar dilution test. C: *Cebo* ecotype; M: *Manteca* ecotype; L: *Leche* ecotype.

The inhibitory concentrations (IC_{50}) of the most promising extracts, those with MGI higher than 50% at 1000 µg/mL were determined using a standard dose-response model, yielding values ranging from 199 to 688 µg/mL. Notably, the UN310 extract exhibited the highest antifungal activity, with an IC_{50} of 362 µg/mL against *F. equiseti* and 204 µg/mL against *F. solani*. These values were not significantly different from those of the UN93 extract, which displayed an IC_{50} of 200 µg/mL against *F. solani*. In contrast, the endophytic fungus UN51 demonstrated the weakest antifungal activity, with an IC_{50} exceeding 3000 µg/mL against both *Fusarium* pathogens (Table 3).

Table 3. Dose-response curves and median inhibitory concentration (IC_{50}) values of EtOAc extracts which showed % MGI >50% on *Fusarium* phytopathogens.

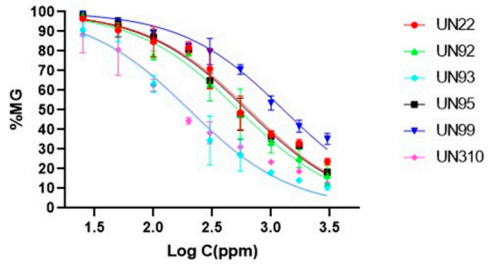

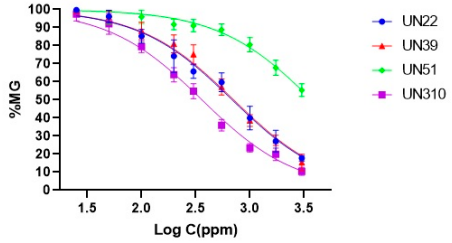

Endophytic EtOAc N.	*F. solani*	*F. equiseti*
	IC_{50} (µg/mL)	IC_{50} (µg/mL)
UN22	650 ± 69^{b,B}	688 ± 50^{a,B}
UN39	N/D	710 ± 43^{a}
UN51	N/D	>3000
UN92	531 ± 51^{b}	N/D
UN93	**199 ± 29^{c}**	N/D
UN95	550 ± 40^{b}	N/D
UN99	1281 ± 78^{a}	N/D
UN310	**204 ± 25^{c,D}**	**362 ± 27^{b,D}**

Values followed by the same lowercase letters in the columns of % MGI for each pathogen at 1000 µg/mL do not show significant differences according to Tukey's test ($p > 0.05$). Similarly, means followed by the same uppercase letters in the rows are not significantly different in a one-way ANOVA analysis ($p > 0.05$).

3.3. Morphological and Molecular Characterizations of the Most Promising Endophytes

Figure 3 illustrates the macroscopic characteristics of the eight selected endophytic strains cultured on PDA. Colonies of UN22, UN39, UN92, UN93, UN95, UN99, and UN310 exhibited white

 doi:10.20944/preprints202512.0969.v1

to gray, woolly aerial mycelium, accompanied by yellow-orange exudates and a dark gray to black reverse pigmentation, with distinct lobed margins. In contrast, strain UN51 displayed the most divergent macroscopic features forming a colony with entire margins, a light-yellow velvety mycelium, and occasional dark brown exudates.

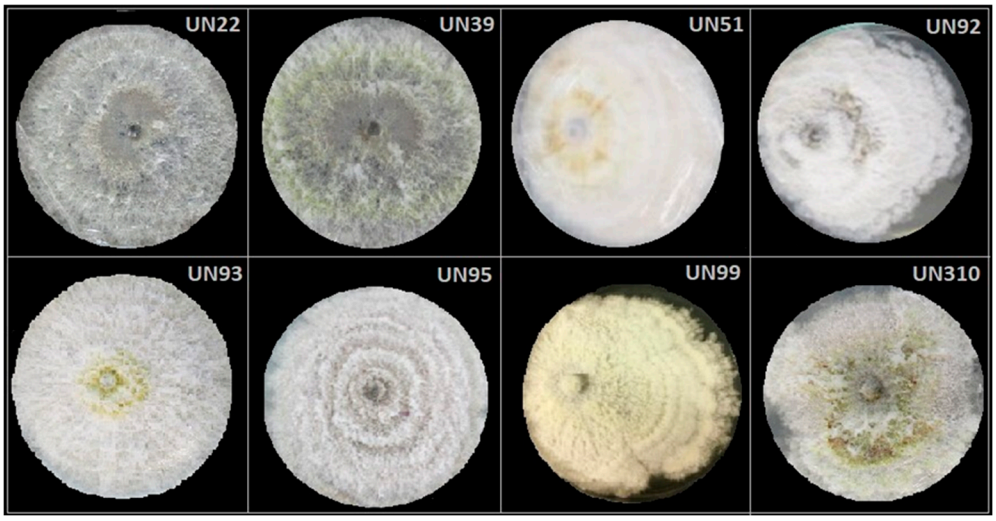

Figure 3. Macroscopic features of selected antifungal endophytes. Pictures were taken on PDA plates at 14th day of culture.

A significant challenge in endophytic fungal identification is the absence of conidia or other reproductive structures when cultured in conventional media, as widely reported in scientific literature [59]. To overcome this limitation, molecular characterization was performed on the eight selected endophytes. Sequence analysis revealed a 99–100% similarity with previously deposited sequences in GenBank, except for strain UN51, which exhibited 96% correspondence (Table 4). All strains coded as UN22, UN39, UN92, UN93, UN95, UN99, and UN310 were closely related to species of the genus *Diaporthe*. In contrast, strain UN51 was more distantly and showed greater similarity to the ITS1 region of species within the genus *Nodulisporium* (Figure 3). Given its IC_{50} value, UN51 was reclassified as an inactive endophytic strain against *F. solani* and *F. equiseti.*

Table 4. Identification of active endophytic fungi isolated from Antillean avocado leaves.

Fungal isolate	Accession number	Closest related species	Similarity (%)
UN22	OQ914368	MW566594.1 *Diaporthe ueckeri*	99
UN39	OQ914369	MW380843.1 *Diaporthe phaseolorum*	100
UN51	OQ914370	EF694672.1 *Nodulisporium sp.*	96
UN92	OQ914371	MW380843.1 *Diaporthe phaseolorum*	100
UN93	OQ914372	KF498865.1 *Diaporthe phaseolorum*	100
UN95	OQ914373	KX631735.1 *Diaporthe longicolla*	100
UN99	OQ914374	AY577815.1 *Diaporthe phaseolorum*	100
UN310	OQ914375	KF498865.1 *Diaporthe phaseolorum*	99

3.4. Some Antifungal Compounds from Endophytic Diaporthe sp.

Notably, the endophytic isolates exhibiting the highest antifungal activity against *F. solani* and *F. equiseti* were phylogenetically related with the genus *Diaporthe* (Table 4). This genus, classified within the *phylum* Ascomycota, comprises over 950 described species that function as endophytes, saprophytes, or pathogens in a diverse range of plant and mammalian hosts [8]. Species within this

 doi:10.20944/preprints202512.0969.v1

genus are characterized by their ability to produce a broad spectrum of bioactive metabolites, including terpenoids, steroids, macrolides, alkaloids, flavonoids, and polyketides [60]. These metabolites exhibit cytotoxic and antineoplastic effects [61], anti-inflammatory [62], hypocholesterolemic [63], cytotoxic [64], herbicide [65], antibacterial and antifungal activities [66].

Among antifungal metabolites, cytochalasin-like compounds are the most abundant in *Diaporthe* genus (Figure 4). These secondary metabolites, derived from polyketide-amino acid fusion, have demonstrated biocontrol potential. They are known as microfilament targeting molecules which exhibit a wide range of biological activities, by interfering with several cellular processes involving cytoskeleton formation [67]. For example, Huang et al. reported the cytochalasins E (**1**), H (**2**), and 7-acetoxy-cytochalasin (**3**) from *Diaporthe sp*., exhibiting strong antifungal activity against *Alternaria oleracea, Pestalotiopsis theae*, and *Colletotrichum capsici* (MIC= 3.125–12.5 μg/mL) [68]. Similarly, cytochalasin H (**2**), N (**4**), and epoxy-cytochalasin H (**5**) from *Phomopsis sp.* By254 inhibited *Sclerotinia sclerotiorum, Fusarium oxysporum, Botrytis cinerea*, and *Rhizoctonia cerealis* (IC_{50}= 0.1–5.0 μg/mL). [69] In addition, cytochalasin J (**6**) from *D. miriciae* showed antifungal activity against the fungal plant pathogens *Phomopsis obscurans* and *P. viticola* at 300 μM. [70]

Diaporthe species produce another important antifungal compounds that had been evaluated on plant phytopathogens (Figure 4). Among them, phomompsolide A (**7**), phomopsolide B (**8**) and phomopsolide C (**9**), isolated from *D. maritima* cultures, demostrated growth inhibition on *Microbotryum violaceum* and *Saccharomyces cerevisiae* at 25-250 μM. [71] Likewise, phomopsolide G (**10**) was isolated from *Diaporthe sp.* AC1 and showed moderate antifungal activity against *Fusarium graminearum*, *F. moniliforme,* and *Botrytis cinerea*. [72] Additionally, the monoterpene verbanol (**11**) from *D. terebinthifolii* showed inhibitory activity on the germination of *Phyllosticta citricarpa* conidia. [73] In the same way, two xanthone dimers, diaporxanthone A (**12**) and diaporxanthone B (**13**), produced by *D. goulteri* L17 exhibited moderate antifungal activities against *Nectria sp.* and *Colletotrichum musae.* [74] Gao *et.al* (2020) isolated from *D. eucalyptorum* a rare polyketide fatty acid, eucalyptacid A (**14**),with MIC values ranging from 12.5-50.0 μM against *Alternaria solani, B. cinerea, F. solani,* and *Gibberella saubinettii*. [75] The dihydroisocoumarin (−)-(3R,4R)-*cis*-4-hydroxy-5-methylmellein (**15**) produced by *D. cf. heveae,* drastically reduced the growth of *Phyllosticta citricarpa* and *Colletotrichum abscissum*, two important citrus diseases worldwide. [76]

3.5. Molecular Docking of Diaporthe Antifungals with Chitin Synthase

The amino acid sequences of CS for *F. solani* and *F. equiseti* were retrieved from the UniProt database under accession codes A0A9P9GUZ8 and A0A8J2II09, respectively. A BLASTp search against the PDB identified the cryo-EM structure of *Phytophthora sojae* chitin synthase 1 (PDB ID: 7WJO) as the most suitable template for homology modeling, given its high sequence identity and structural coverage. Among the 3D models generated by the different servers, those predicted by Robetta exhibited the highest structural fidelity to the template, displaying the lowest Root Mean Square Deviation (RMSD) values of 1.68 Å for *F. equiseti* and 2.21 Å for *F. solani*. Consequently, these Robetta-derived models were selected as the reference structures for the subsequent molecular docking simulations.

 doi:10.20944/preprints202512.0969.v1

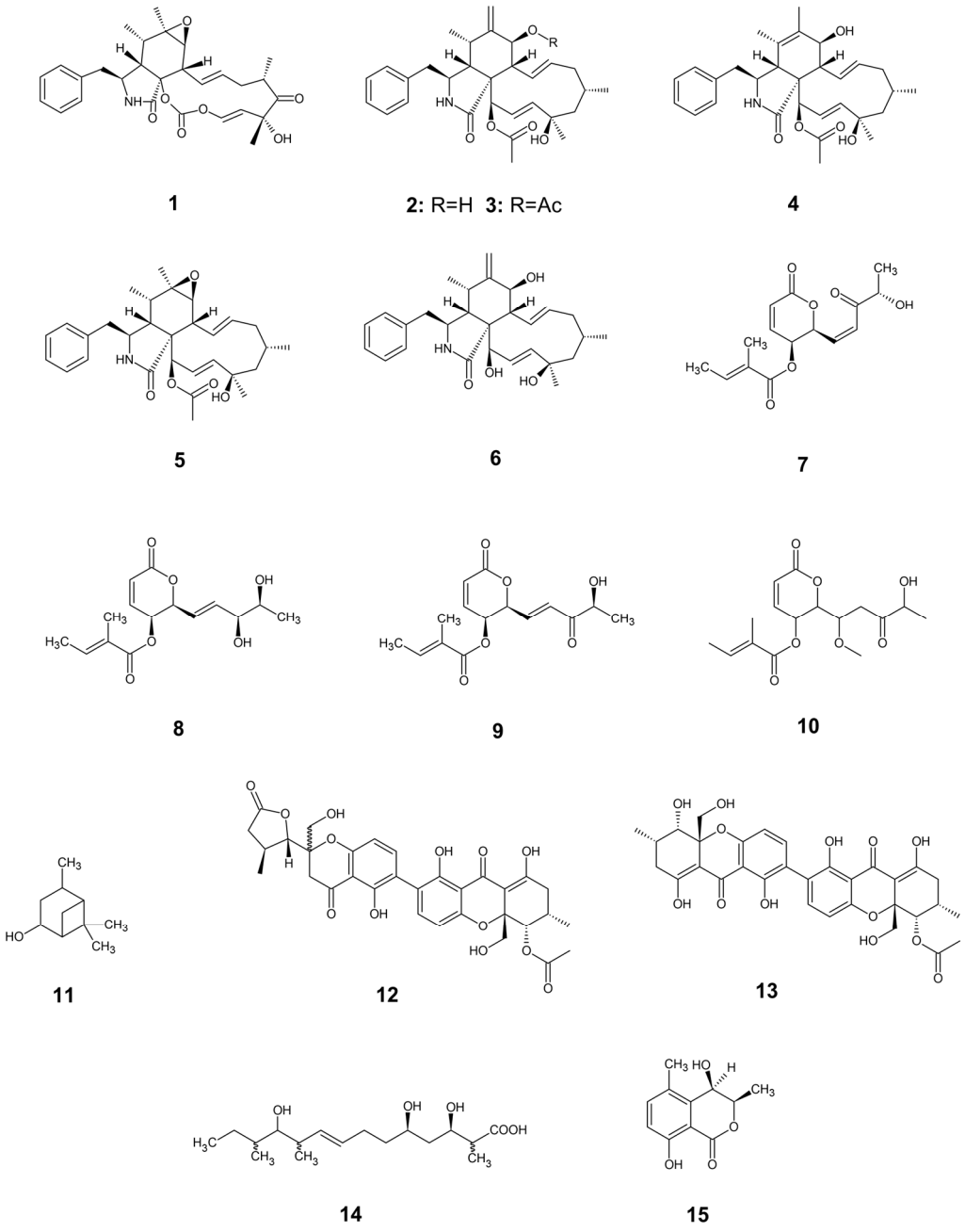

Figure 4. Antifungal metabolites from *Diaporthe sp.* with inhibitory activity on plant phytopathogens.

Visual inspection of the superimposed structures confirms a remarkable topological similarity between the generated *Fusarium* models and the *P. sojae* template. Crucially, the detailed analysis of the active site reveals that the architecture of the ligand-binding pocket is maintained in both *F. solani* and *F. equiseti* models. As depicted in Figure 5, the key amino acid residues responsible for stabilizing the reference inhibitor Nikkomycin Z are spatially conserved. This structural preservation suggests that the generated models possess a binding pocket competent for ligand recognition, thereby validating their use for the subsequent molecular docking of the endophytic metabolites.

 doi:10.20944/preprints202512.0969.v1

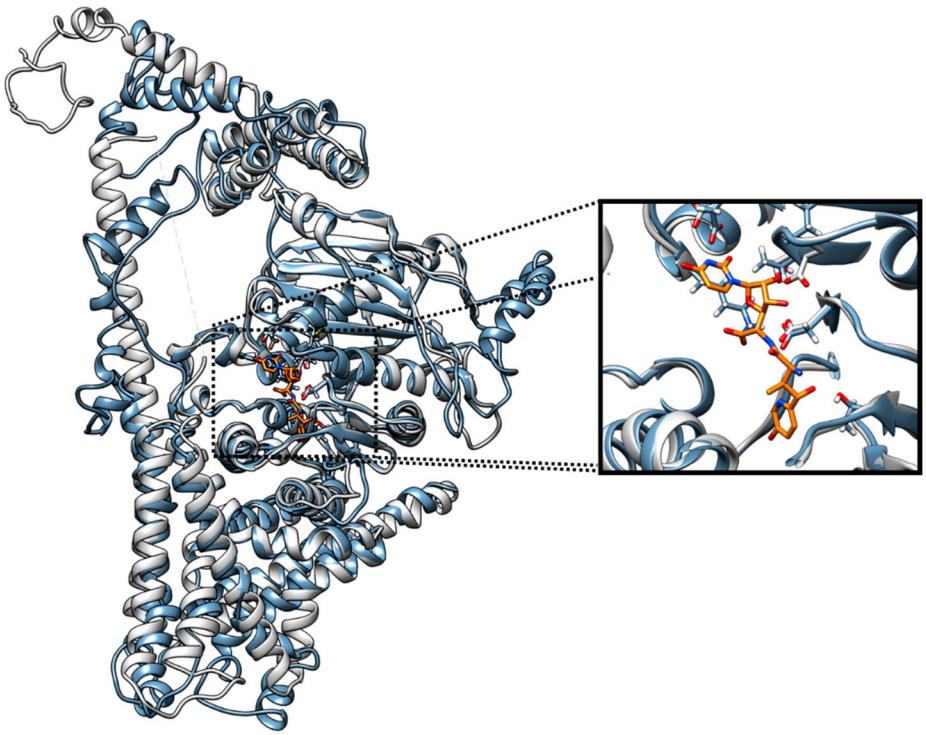

Figure 5. Global superimposition of the generated *F. equiseti* CS model against the *P. sojae* template (PDB: 7WJO). Grey structure displays the CS template (*P. sojae*) and blue displays *F. equiseti* model. At right part of the picture a zoom of binding zone is shown.

The normalized binding energy values (Vina score) shown in Table 5 revealed that several isolated metabolites possess a theoretical affinity for the CS active site that rivals or even surpasses the reference inhibitor. Notably, compound **12** exhibited the highest predicted binding stability, achieving a normalized Vina score of 1.0 in *F. equiseti* and 0.83 in *F. solani*. These values suggest that compound **12** has the potential to form a complex with the enzyme that is theoretically more favorable than the control Nikkomycin Z (which scored 0.65 and 0.57, respectively). This predictive data implies that the hydrophobic skeleton of the isolated endophytes metabolites likely fits tightly within the catalytic pocket, potentially driven by strong Van der Waals interactions.

Table 5. Scoring table of molecular docking simulations of each metabolite against the CS *F. solani* and *F. equiseti*. In Consensus score column green color displays the best scores and red color the worst scores.

	F. solani			*F. equiseti*		
id	Vina score	PROLIF similarity	Consensus score	Vina score	PROLIF similarity	Consensus score
Nikkomycin Z	0,57	1,00	0,78	0,65	1,00	0,82
Cytochalasin E (**1**)	0,27	0,63	0,45	0,37	0,48	0,42
Cytochalasin H (**2**)	0,16	0,49	0,32	0,30	0,38	0,34
7-acetoxy-cytochalasin (**3**)	0,22	0,75	0,49	0,26	0,85	0,56
Cytochalasin N (**4**)	0,24	0,44	0,34	0,38	0,75	0,57
Epoxy-cytochalasin H (**5**)	0,26	0,67	0,46	0,29	0,57	0,43
Cytochalasin J (**6**)	0,23	0,69	0,46	0,38	0,59	0,48
Phomompsolide A (**7**)	0,31	0,42	0,37	0,37	0,55	0,46
Phomompsolide B (**8**)	0,40	0,56	0,48	0,24	0,55	0,39
Phomompsolide C (**9**)	0,34	0,51	0,43	0,25	0,49	0,37
Phomompsolide G (**10**)	0,16	0,19	0,17	0,33	0,45	0,39
Verbanol (**11**)	0,00	0,28	0,14	0,00	0,51	0,26

 doi:10.20944/preprints202512.0969.v1

Diaporxanthone A (**12**)	1,00	0,22	0,61	0,96	0,50	0,73
Diaporxanthone B (**13**)	0,71	0,29	0,50	1,00	0,45	0,72
Eucalyptacid A (**14**)	0,04	0,00	0,02	0,41	0,00	0,20
Dihydroisocoumarin (−)-(3R,4R)-cis-4-hydroxy-5-methylmellein (**15**)	0,18	0,14	0,16	0,18	0,46	0,32

While high affinity is crucial, the specific mode of binding determines the biological outcome. The interaction fingerprint analysis (PLIF) quantified how well the candidates mimicked the key contacts established by Nikkomycin Z. The similarity scores for the top candidates ranged between 0.40 and 0.66. While lower than the control (which is 1.0 by definition), these values are significant for non-peptidic small molecules. Specifically, compound **13** showed the highest structural similarity in interaction patterns against *F. equiseti* (0.66), implying that it engages conserved residues essential for catalysis, such as those involved in uridine binding or translocation. [77,78] The lower similarity scores observed for compound **12** (approx. 0.40–0.46), despite its high energy, suggest it may occupy the binding pocket in a unique orientation, potentially exploiting auxiliary sub-pockets not accessed by the reference inhibitor.

Detailed inspection of the ligand-receptor contacts in *F. equiseti* reveals that Nikkomycin Z (NZ), anchors itself within the active site through hydrogen bonds with Asp388, Pro462, and Ala464, while relying on a critical hydrophobic stacking interaction with Trp553 as is show in Figure 6. This tryptophan residue is structurally significant, as it corresponds to the conserved aromatic residues found in the catalytic loop of the *P. sojae* template and other Family 2 glycosyltransferases, acting as a gatekeeper that stabilizes the GlcNAc sugar ring. [22,79] Notably, compound **12** successfully mimics this pharmacophoric feature, preserving the hydrophobic clamp with Trp553 and the hydrogen bond with Pro462, while further stabilizing the complex through additional hydrogen bonds with Asp538 and Gly390. The engagement with Asp538 is particularly relevant, as aspartate residues in this region are typically involved in coordinating the divalent metal ions essential for catalysis. [80,81]

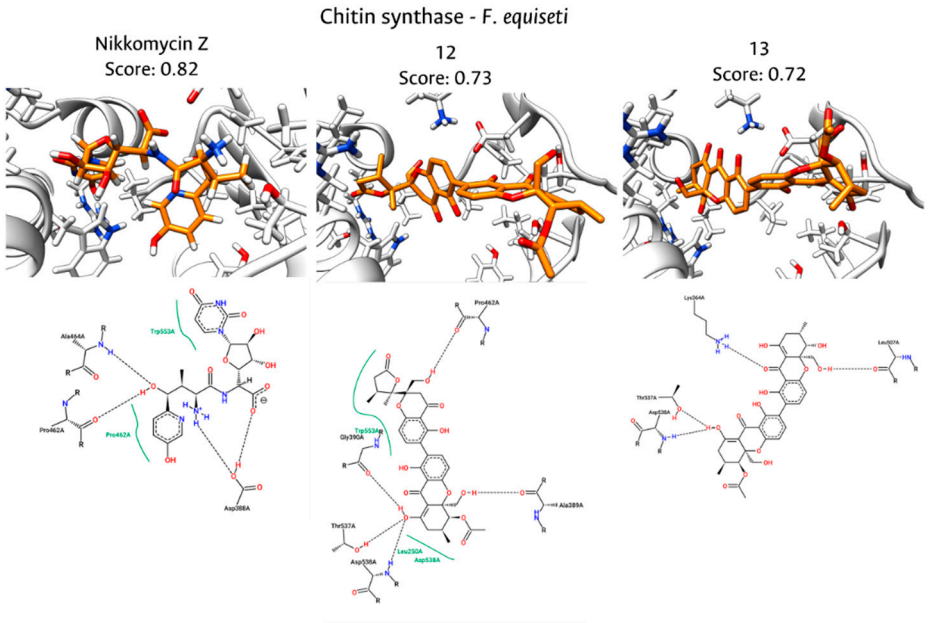

Figure 6. Interactions between binding site of chitin synthase of *F. equiseti* and docked molecules (NikkomycinZ, compounds **12** and **13**). In the upper part is displayed the 3D interactions and in the lower part the 2D interactions plots.

The structural basis for the consensus ranking becomes evident when comparing these interaction profiles. While compound **13** establishes a strong hydrogen bonding network involving Asp538, Thr537, and Lys364, it notably lacks the hydrophobic interaction with Trp553 observed in

 doi:10.20944/preprints202512.0969.v1

both NZ and compound **12**. This absence likely accounts for its slightly lower thermodynamic stability (Vina score) compared to compound **12**, despite having a high interaction similarity index. Consequently, compound **12** could have a better activity (Consensus Score = 0.73) because it acts as a dual-modality inhibitor: it not only occupies the catalytic center by interacting with essential aspartates but also replicates the hydrophobic stabilization mechanism exploited by the reference inhibitor.

The docking results for *F. solani* reveal a distinct interaction landscape, likely attributed to the greater structural divergence of its catalytic domain relative to the template. This conformational variability is reflected in the binding mode of Nikkomycin Z, which shifts to a pose dominated by hydrogen bonds with Asp510, Gln549, Thr537, and Ala464, notably losing the strong hydrophobic anchor observed in the *F. equiseti* model as is displayed in Figure 7. In contrast, compound **12** demonstrates remarkable adaptability to this distorted pocket. It not only establishes a wide hydrogen bonding network with Pro462, Thr537, Asp538, Ala389, and Gly690, but crucially, it recovers the hydrophobic stacking interaction with Trp553. This ability explains the predicted binding energy (0.83 and 0.57 for compound **12** and Nikkomycin respectively).

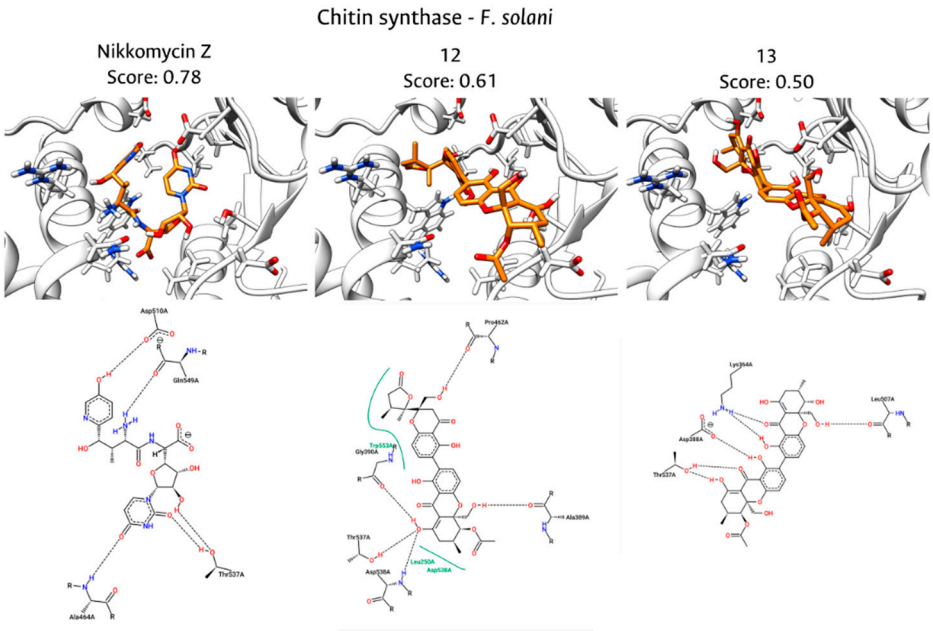

Figure 7. Interactions between binding site of chitin synthase of *F. solani* and docked molecules (NikkomycinZ, compounds **12** and **13**). In the upper part is displayed the 3D interactions and in the lower part the 2D interactions plots.

Compound **13** relies primarily on electrostatic and polar stabilization, anchoring to the active site through hydrogen bonds with Lys364, Asp388, and Thr537. While Thr537 emerges as persistent contact across all ligands, suggesting a pivotal role in substrate orientation, the absence of the hydrophobic clamp with Trp553 limits the binding stability of compound **13**. This comparison further validates the consensus scoring hierarchy, identifying compound **12** as the most robust candidate capable of maintaining key inhibitory interactions despite the structural plasticity of the pathogen's target site for chitin synthase in both organisms.

3.6. Concluding Remarks

Antillean avocado trees that survived adverse phytosanitary conditions in Montes de María serve as reservoirs of diverse endophytic fungi, some capable of producing antifungal metabolites against *F. solani* and *F. equiseti*. The most active isolates were found in Manteca and Cebo ecotypes, suggesting a potential correlation between endophyte presence and host resilience. Molecular

 doi:10.20944/preprints202512.0969.v1

analyses identified these isolates as *Diaporthe* species, a genus renowned for its production of bioactive secondary metabolites. Notably, crude extracts from *Diaporthe sp.* strains UN93 and UN310 demonstrated significant antifungal activity, with IC_{50} values near 200 µg/mL against *Fusarium spp*.

This study also identified *Epicoccum sp.* and *Colletotrichum sp.* in the secondary roots of symptomatic avocado trees, with *Fusarium sp.* being the most prevalent. No *Phytophthora* species were isolated, possibly due to their specific growth requirements, though their absence cannot be confirmed. Future research should expand microbiome characterization using genetic sequencing. In addition, the validation of *in vitro* results through controlled seedling experiments is crucial, as antagonistic effects do not always translate to effective disease control. The challenges in studying the pathosystem open the door to an alternative biocontrol strategy: the direct application of chemical compounds produced by endophytic microorganisms to protect their host against biotic and abiotic stress factors. Thus, further studies should focus on the chemical characterization of promising extracts to identify the bioactive compounds responsible for their antifungal activity and assess their potential applications in plant disease management.

Furthermore, the integrated *in silico* analysis proposes a plausible molecular mechanism of action, identifying chitin synthase as a potential target for the bioactive metabolites, particularly candidates **12** and **13**. However, these computational findings must be interpreted with caution, as they rely on homology models that, despite their structural quality, inherently carry a degree of uncertainty regarding the precise conformational landscape of the native enzymes. Consequently, these predictive results should be viewed as a theoretical framework to guide future molecular exploration. Subsequent investigations must prioritize direct enzymatic inhibition assays to experimentally validate the affinity of these molecules; alongside structural biology efforts aimed at crystallizing the specific *Fusarium* CS to corroborate the binding modes proposed in this study.

Supplementary Materials: The following supporting information can be downloaded at the website of this paper posted on Preprints.org, Table S1: DNA sequences for ITS1 region of *Fusarium* pathogens and promising endophytes; Table S2: Extraction yields for antifungal endophytes fermentation using EtOAc.

Author Contributions: Angie T. Robayo-Medina: Investigation, data curation, formal analysis, writing—original draft preparation; Katheryn-Michell Camargo-Jimenez: Investigation; Felipe Victoria-Muñoz: Computational study, writing—original draft preparation; Wilman Delgado-Avila: conceptualization; Luis Cuca Suarez: supervision. Monica Ávila-Murillo: writing—review and editing, project administration, funding acquisition. All experimental section was executed by Universidad Nacional de Colombia and computational study by Fundación Universitaria Salesiana.

Funding: This work was financially supported by Ministerio de Ciencia, Tecnología e Innovación de Colombia: "*Fondo nacional de financiamiento para la ciencia, la tecnología y la innovación, Fondo Francisco José De Caldas*" contrato 80740-159-2021; Dirección de Investigación y Extensión Sede Bogotá, Universidad Nacional de Colombia, HERMES Project Codes 48477 and 51310; Facultad de Ciencias, Sede Bogotá, Universidad Nacional de Colombia, HERMES Project Code 50092, and the APC was funded 50 percent by Fundación Universitaria Salesiana and 50 percent by the authors.

Data Availability Statement: The authors declare that the data supporting the findings of this study are available within the paper and its Supplementary Information files. Should any raw data files be needed in another format they are available from the corresponding author upon reasonable request.

Acknowledgments: The authors thanks to Asociación de Productores de Aguacate Tecnificado de los Montes de Maria (ASPROATEMON) for their technical guide in sampling Antillean avocado ecotypes.

Conflicts of Interest: The authors declare no conflicts of interest.

 doi:10.20944/preprints202512.0969.v1

Abbreviations

The following abbreviations are used in this manuscript:

AWC	Avocado Wilt Complex
CS	Chitin Synthase
DMSO	Dimethyl Sulfoxide
EtOAc	Ethyl Acetate
IC_{50}	Median Inhibitory Concentration
MGI	Mycelial Growth Inhibition
MIC	Minimal Inhibitory Concentration
PDA	Potato Dextrose Agar

References

1. M. Hafez, M. Telfer, S. Chatterton, and R. Aboukhaddour, "Specific Detection and Quantification of Major Fusarium spp. Associated with Cereal and Pulse Crops," in *Plant-Pathogen Interactions*, vol. 2659, New York: Humana, New York, NY, 2023, pp. 1–21. doi: 10.1007/978-1-0716-3159-1_1.
2. L. Zakaria, "Fusarium Species Associated with Diseases of Major Tropical Fruit Crops," *Horticulturae*, vol. 9, no. 3, p. 322, Mar. 2023, doi: 10.3390/horticulturae9030322.
3. T. I. Ekwomadu, S. A. Akinola, and M. Mwanza, "Fusarium mycotoxins, their metabolites (Free, emerging, and masked), food safety concerns, and health impacts," *Int J Environ Res Public Health*, vol. 18, no. 22, Nov. 2021, doi: 10.3390/ijerph182211741.
4. D. Huang *et al.*, "The epigenetic mechanisms in Fusarium mycotoxins induced toxicities," *Food and Chemical Toxicology*, vol. 123, pp. 595–601, 2019, doi: 10.1016/j.fct.2018.10.059.
5. D. P. Clements and E. A. Bihn, "Safety and Practice for Organic Food," in *Safety and Practice for Organic Food*, Elsevier Inc., 2019, ch. The Impact, pp. 321–344. doi: 10.1016/B978-0-12-812060-6.00016-7.
6. M. Tör and A. Woods-Tör, "Genetic Modification of Disease Resistance : Fungal and Oomycete Pathogens," *Encyclopedia of Applied Plant Sciences*, vol. 3, pp. 83–87, 2017, doi: 10.1016/B978-0-12-394807-6.00054-X.
7. P. Koli, N. R. Bhardwaj, and S. K. Mahawer, "Climate Change and Agricultural Ecosystems," in *Climate Change and Agricultural Ecosystems*, Elsevier Inc., 2019, ch. Agrochemic, pp. 65–94. doi: 10.1016/B978-0-12-816483-9.00004-9.
8. S. Hilário and M. F. M. Gonçalves, "Endophytic Diaporthe as Promising Leads for the Development of Biopesticides and Biofertilizers for a Sustainable Agriculture," Dec. 01, 2022, *MDPI*. doi: 10.3390/microorganisms10122453.
9. A. Sharma, N. Kaushik, A. Sharma, T. Marzouk, and N. Djébali, "Exploring the potential of endophytes and their metabolites for bio-control activity," *3 Biotech*, vol. 12, no. 10, p. 277, Oct. 2022, doi: 10.1007/s13205-022-03321-0.
10. S. Mishra, Priyanka, and S. Sharma, "Metabolomic Insights Into Endophyte-Derived Bioactive Compounds," Mar. 02, 2022, *Frontiers Media S.A.* doi: 10.3389/fmicb.2022.835931.
11. J. G. Harrison and E. A. Griffin, "The diversity and distribution of endophytes across biomes, plant phylogeny and host tissues: how far have we come and where do we go from here?," *Environ Microbiol*, vol. 22, no. 6, pp. 2107–2123, Jun. 2020, doi: 10.1111/1462-2920.14968.
12. G. Strobel and B. Daisy, "Bioprospecting for Microbial Endophytes and Their Natural Products," *Microbiology and Molecular Biology Reviews*, vol. 67, no. 4, pp. 491–502, Dec. 2003, doi: 10.1128/MMBR.67.4.491-502.2003.
13. O. Burbano-Figueroa, "West Indian avocado agroforestry systems in Montes de María (Colombia): a conceptual model of the production system," *Rev Chapingo Ser Hortic*, vol. 25, no. 2, pp. 75–102, 2019, doi: 10.5154/r.rchsh.2018.09.018.
14. J. Y. Vega, "El aguacate en Colombia : Estudio de caso de los Montes de María, en el Caribe colombiano," *Banco de la República de Colombia. Centro de estudios económicos regionales.*, vol. 171, pp. 1–35, Aug. 2012, doi: 10.32468/dtseru.171.
15. A. Puello, "La transformación de la estructura productiva de los Montes de María: de despensa agrícola a distrito minero-energético," *Revista Digital de Historia y Arqueología desde el Caribe*, vol. 29, pp. 52–83, 2016.

 doi:10.20944/preprints202512.0969.v1

16. J. G. Ramírez-Gil, "Avocado wilt complex disease, implications and management in Colombia," *Revista Facultad Nacional de Agronomía*, vol. 71, no. 2, pp. 8525–8541, 2018, doi: 10.15446/rfna.v71n2.66465.
17. X. Zou *et al.*, "ROS Stress and Cell Membrane Disruption are the Main Antifungal Mechanisms of 2-Phenylethanol against Botrytis cinerea," *J Agric Food Chem*, vol. 70, no. 45, pp. 14468–14479, Nov. 2022, doi: 10.1021/ACS.JAFC.2C06187.
18. S. Oiki, R. Nasuno, S. ichi Urayama, H. Takagi, and D. Hagiwara, "Intracellular production of reactive oxygen species and a DAF-FM-related compound in Aspergillus fumigatus in response to antifungal agent exposure," *Scientific Reports 2022 12:1*, vol. 12, no. 1, pp. 13516-, Aug. 2022, doi: 10.1038/s41598-022-17462-y.
19. S. Hasim and J. J. Coleman, "Targeting the fungal cell wall: current therapies and implications for development of alternative antifungal agents," *Future Med Chem*, vol. 11, no. 8, p. 869, Apr. 2019, doi: 10.4155/FMC-2018-0465.
20. S. L. Lima, A. L. Colombo, and J. N. de Almeida Junior, "Fungal Cell Wall: Emerging Antifungals and Drug Resistance," *Front Microbiol*, vol. 10, p. 492317, Nov. 2019, doi: 10.3389/FMICB.2019.02573/ENDNOTE.
21. S. M. Bowman and S. J. Free, "The structure and synthesis of the fungal cell wall," *Bioessays*, vol. 28, no. 8, pp. 799–808, Aug. 2006, doi: 10.1002/BIES.20441.
22. Y. Wu *et al.*, "Structures and mechanism of chitin synthase and its inhibition by antifungal drug Nikkomycin Z," *Cell Discov*, vol. 8, no. 1, pp. 129-, Dec. 2022, doi: 10.1038/S41421-022-00495-Y;SUBJMETA.
23. X. Shi, S. Qiu, Y. Bao, H. Chen, Y. Lu, and X. Chen, "Screening and Application of Chitin Synthase Inhibitors," *Processes 2020, Vol. 8, Page 1029*, vol. 8, no. 9, p. 1029, Aug. 2020, doi: 10.3390/PR8091029.
24. K. Waheeda and K. Shyam, "Formulation of Novel Surface Sterilization Method and Culture Media for the Isolation of Endophytic Actinomycetes from Medicinal Plants and its Antibacterial Activity," *J Plant Pathol Microbiol*, vol. 08, no. 02, pp. 1–9, 2017, doi: 10.4172/2157-7471.1000399.
25. X. Yang *et al.*, "Identification, Pathogenicity, and Genetic Diversity of Fusarium spp. Associated with Maize Sheath Rot in Heilongjiang Province, China," *Int J Mol Sci*, vol. 23, no. 18, Sep. 2022, doi: 10.3390/ijms231810821.
26. L. E. Parkinson, R. G. Shivas, and E. K. Dann, "Pathogenicity of nectriaceous fungi on avocado in Australia," *Phytopathology*, vol. 107, no. 12, pp. 1479–1485, 2017, doi: 10.1094/PHYTO-03-17-0084-R.
27. M. A. Gamboa, S. Laureano, and P. Bayman, "Measuring diversity of endophytic fungi in leaf fragments: Does size matter?," *Mycopathologia*, vol. 156, no. 1, pp. 41–45, 2003, doi: 10.1023/A:1021362217723.
28. C. Brunner-Mendoza, H. Navarro-Barranco, M. A. Ayala-zermeño, M. Mellín-Rosas, and C. Toriello, "Obtención y caracterización de cultivos monospóricos de Metarhizium anisopliae (Hypocreales: Clavicipitaceae) para genotipificación," in *Memorias del XXXVI Congreso Nacional de Control Biológico*, Oaxaca de Juárez, 2013, pp. 52–55.
29. X. Hu, G. Webster, L. Xie, C. Yu, Y. Li, and X. Liao, "A new method for the preservation of axenic fungal cultures," *J Microbiol Methods*, vol. 99, no. 1, pp. 81–83, 2014, doi: 10.1016/j.mimet.2014.02.009.
30. E. Terhonen, N. Sipari, and F. O. Asiegbu, "Inhibition of phytopathogens by fungal root endophytes of Norway spruce," *Biological Control*, vol. 99, pp. 53–63, 2016, doi: 10.1016/j.biocontrol.2016.04.006.
31. J. E. Parra Amin, L. E. Cuca, and A. González-Coloma, "Antifungal and phytotoxic activity of benzoic acid derivatives from inflorescences of Piper cumanense," *Nat Prod Res*, vol. 35, no. 16, pp. 2763–2771, 2021, doi: 10.1080/14786419.2019.1662010.
32. A. E. Arnold, "Understanding the diversity of foliar endophytic fungi: progress, challenges, and frontiers," *Fungal Biol Rev*, vol. 21, no. 2–3, pp. 51–66, May 2007, doi: 10.1016/j.fbr.2007.05.003.
33. A. Morgulis, G. Coulouris, Y. Raytselis, T. L. Madden, R. Agarwala, and A. A. Schäffer, "Database indexing for production MegaBLAST searches," *Bioinformatics*, vol. 24, no. 16, pp. 1757–1764, Aug. 2008, doi: 10.1093/bioinformatics/btn322.
34. A. Bateman, "UniProt: a worldwide hub of protein knowledge," *Nucleic Acids Res*, vol. 47, no. D1, pp. D506–D515, Jan. 2019, doi: 10.1093/NAR/GKY1049.
35. S. Ovchinnikov, H. Park, D. E. Kim, F. DiMaio, and D. Baker, "Protein structure prediction using Rosetta in CASP12," *Proteins: Structure, Function and Bioinformatics*, vol. 86, pp. 113–121, Mar. 2018, doi: 10.1002/PROT.25390;REQUESTEDJOURNAL:JOURNAL:10970134;WGROUP:STRING:PUBLICATION.

 doi:10.20944/preprints202512.0969.v1

36. J. Jumper *et al.*, "Highly accurate protein structure prediction with AlphaFold," *Nature 2021 596:7873*, vol. 596, no. 7873, pp. 583–589, Jul. 2021, doi: 10.1038/s41586-021-03819-2.
37. W. Zheng *et al.*, "Deep-learning-based single-domain and multidomain protein structure prediction with D-I-TASSER," *Nature Biotechnology 2025*, pp. 1–13, May 2025, doi: 10.1038/s41587-025-02654-4.
38. O. Trott and A. J. Olson, "AutoDock Vina: Improving the speed and accuracy of docking with a new scoring function, efficient optimization, and multithreading," *J Comput Chem*, vol. 31, no. 2, pp. 455–461, Jan. 2010, doi: 10.1002/JCC.21334;CTYPE:STRING:JOURNAL.
39. E. Jurrus *et al.*, "Improvements to the APBS biomolecular solvation software suite," *Protein Sci*, vol. 27, no. 1, pp. 112–128, Jan. 2018, doi: 10.1002/PRO.3280.
40. G. Landrum, "Release 2016_09_4 (Q3 2016) Release · rdkit/rdkit · GitHub." Accessed: Dec. 02, 2025. [Online]. Available: https://github.com/rdkit/rdkit/releases/tag/Release_2016_09_4
41. N. M. O'Boyle, M. Banck, C. A. James, C. Morley, T. Vandermeersch, and G. R. Hutchison, "Open Babel: An open chemical toolbox," *Journal of Cheminformatics 2011 3:1*, vol. 3, no. 1, pp. 33-, Oct. 2011, doi: 10.1186/1758-2946-3-33.
42. W. Chen *et al.*, "Structural basis for directional chitin biosynthesis," *Nature 2022 610:7931*, vol. 610, no. 7931, pp. 402–408, Sep. 2022, doi: 10.1038/s41586-022-05244-5.
43. R. Meli and P. C. Biggin, "spyrmsd: symmetry-corrected RMSD calculations in Python," *Journal of Cheminformatics 2020 12:1*, vol. 12, no. 1, pp. 49-, Aug. 2020, doi: 10.1186/S13321-020-00455-2.
44. C. Bouysset and S. Fiorucci, "ProLIF: a library to encode molecular interactions as fingerprints," *Journal of Cheminformatics 2021 13:1*, vol. 13, no. 1, pp. 72-, Sep. 2021, doi: 10.1186/S13321-021-00548-6.
45. M. Ajmal, A. Hussain, A. Ali, H. Chen, and H. Lin, "Strategies for Controlling the Sporulation in Fusarium spp.," Jan. 01, 2023, *MDPI*. doi: 10.3390/jof9010010.
46. G. G. Olalde-Lira and B. N. Lara-Chávez, "Characterization of Fusarium spp., a Phytopathogen of avocado (Persea americana Miller var. drymifolia (Schltdl. and Cham.) in Michoacán, México," *Rev. FCA UNCUYO*, vol. 52, no. 2, pp. 301–316, 2020.
47. E. K. Wanjiku, J. W. Waceke, B. W. Wanjala, and J. N. Mbaka, "Identification and Pathogenicity of Fungal Pathogens Associated with Stem End Rots of Avocado Fruits in Kenya," *Int J Microbiol*, vol. 2020, 2020, doi: 10.1155/2020/4063697.
48. M. Guerrero Rojas and A. Ramos Portilla, *Prevenga y maneje la pudrición radical del aguacate causada por el Oomycete Phytophthora cinnamomi Rands*. Bogotá D.C., Colombia: Oficina Asesora de Comunicaciones ICA, 2016.
49. D. Orjuela Corchuelo and M. Avila Murillo, "Microorganismos endófitos como alternativa para el control de hongos patógenos asociados al cultivo del aguacate en Colombia," Tesis de Maestria en Ciencias-Química, Universidad Nacional de Colombia, Bogotá D.C., Colombia, 2018.
50. J. G. Ramírez-Gil, E. Gilchrist Ramelli, and J. G. Morales Osorio, "Economic impact of the avocado (cv. Hass) wilt disease complex in Antioquia, Colombia, crops under different technological management levels," *Crop Protection*, vol. 101, pp. 103–115, Nov. 2017, doi: 10.1016/j.cropro.2017.07.023.
51. L. Palacios Joya, "Caracterización de microorganismos asociados a la pudrición de raíces de aguacate Persea americana Mill en viveros del Valle del Cauca, Colombia," Palmira, Colombia, 2021.
52. R. S. Novoa-Yánez et al., Manual de producción de semilla de aguacate criollo en vivero en los Montes de María, Primera Edición. Mosquera, Cundinamarca: AGROSAVIA, 2023.
53. R. Shahzad, A. L. Khan, S. Bilal, S. Asaf, and I. Lee, "What Is There in Seeds? Vertically Transmitted Endophytic Resources for Sustainable Improvement in Plant Growth," *Front Plant Sci*, vol. 9, no. 24, pp. 1–10, 2018, doi: 10.3389/fpls.2018.00024.
54. P. Chaudhary, U. Agri, A. Chaudhary, A. Kumar, and G. Kumar, "Endophytes and their potential in biotic stress management and crop production," Oct. 17, 2022, *Frontiers Media S.A.* doi: 10.3389/fmicb.2022.933017.
55. S. Verma, K. Kingsley, M. Bergen, K. Kowalski, and J. White, "Fungal Disease Prevention in Seedlings of Rice (Oryza sativa) and Other Grasses by Growth-Promoting Seed-Associated Endophytic Bacteria from Invasive Phragmites australis," *Microorganisms*, vol. 6, no. 1, p. 21, 2018, doi: 10.3390/microorganisms6010021.

 doi:10.20944/preprints202512.0969.v1

56. J. Liu and G. Liu, "Analysis of Secondary Metabolites from Plant Endophytic Fungi," in *Plant Pathogenic Fungi and Oomycetes: Methods and Protocols, Methods in Molecular Biology*, vol. 1848, 2018, pp. 25–38. doi: 10.1007/978-1-4939-8724-5_3.
57. A. Singh *et al.*, "Phytochemical analysis and antimicrobial activity of an endophytic Fusarium proliferatum (ACQR8), isolated from a folk medicinal plant Cissus quadrangularis L.," *South African Journal of Botany*, vol. 140, pp. 87–94, Aug. 2021, doi: 10.1016/j.sajb.2021.03.004.
58. F. Pan, Z. Q. Liu, Q. Chen, Y. W. Xu, K. Hou, and W. Wu, "Endophytic fungus strain 28 isolated from Houttuynia cordata possesses wide-spectrum antifungal activity," *Brazilian Journal of Microbiology*, vol. 47, no. 2, pp. 480–488, Apr. 2016, doi: 10.1016/j.bjm.2016.01.006.
59. A. K. Verma, S. K. Patel, C. B. Pratap, M. Gangwar, and G. Nath, *Advances in Endophytic Research*. New Delhi: Springer India, 2014. doi: 10.1007/978-81-322-1575-2.
60. T.-C. Xu *et al.*, "Bioactive Secondary Metabolites of the Genus Diaporthe and Anamorph Phomopsis from Terrestrial and Marine Habitats and Endophytes: 2010–2019," *Microorganisms*, vol. 9, no. 2, p. 217, Jan. 2021, doi: 10.3390/microorganisms9020217.
61. R. Kretz *et al.*, "The Effect of Cytochalasans on the Actin Cytoskeleton of Eukaryotic Cells and Preliminary Structure–Activity Relationships," *Biomolecules*, vol. 9, no. 2, p. 73, Feb. 2019, doi: 10.3390/biom9020073.
62. Y. Liu *et al.*, "Cytochalasins and polyketides from the fungus Diaporthe sp. GZU-1021 and their anti-inflammatory activity," *Fitoterapia*, vol. 137, Sep. 2019, doi: 10.1016/j.fitote.2019.104187.
63. M. Patil, R. Patil, S. Mohammad, and V. Maheshwari, "Bioactivities of phenolics-rich fraction from Diaporthe arengae TATW2, an endophytic fungus from Terminalia arjuna (Roxb.)," *Biocatal Agric Biotechnol*, vol. 10, pp. 396–402, Apr. 2017, doi: 10.1016/j.bcab.2017.05.002.
64. H. Cui *et al.*, "Alkaloids from the mangrove endophytic fungus Diaporthe phaseolorum SKS019," *Bioorg Med Chem Lett*, vol. 27, no. 4, pp. 803–807, 2017, doi: 10.1016/j.bmcl.2017.01.029.
65. A. Rossana *et al.*, "Bioherbicide production by Diaporthe sp. isolated from the Brazilian Pampa biome," *Biocatal Agric Biotechnol*, vol. 4, no. 4, pp. 575–578, 2015, doi: 10.1016/j.bcab.2015.09.005.
66. C. Medeiros *et al.*, "Antifungal and antibacterial activity of extracts produced from Diaporthe schini," *J Biotechnol*, vol. 294, pp. 30–37, 2019, doi: 10.1016/j.jbiotec.2019.01.022.
67. H. Zhu *et al.*, "Progress in the Chemistry of Cytochalasans," *Prog Chem Org Nat Prod*, vol. 114, pp. 1–134, 2021, doi: 10.1007/978-3-030-59444-2_1.
68. X. Huang *et al.*, "Cytochalasins from endophytic Diaporthe sp. GDG-118," *Nat Prod Res*, pp. 1–9, 2019, doi: 10.1080/14786419.2019.1700504.
69. J. Fu, Y. Zhou, H. Li, Y. Ye, and J. Guo, "Antifungal metabolites from Phomopsis sp. By254, an endophytic fungus in Gossypium hirsutum," *Afr J Microbiol Res*, vol. 5, no. 10, pp. 1231–1236, 2011, doi: 10.5897/AJMR11.272.
70. C. R. de Carvalho, A. Ferreira-D'Silva, D. E. D.E. Wedge, C. L. Cantrell, and L. H. Rosa, "Antifungal activities of cytochalasins produced by Diaporthe miriciae, an endophytic fungus associated with tropical medicinal plants," *Can J Microbiol.*, vol. 64, no. 11, pp. 835–843, 2018, doi: 10.1139/cjm-2018-0131.
71. J. B. Tanney, D. R. Mcmullin, B. D. Green, J. D. Miller, and K. A. Seifert, "Production of antifungal and antiinsectan metabolites by the Picea endophyte Diaporthe maritima sp. nov," *Fungal Biol*, vol. 120, no. 11, pp. 1448–1457, 2016, doi: 10.1016/j.funbio.2016.05.007.
72. H. Gu, S. Zhang, L. Liu, Z. Yang, F. Zhao, and Y. Tian, "Antimicrobial Potential of Endophytic Fungi From Artemisia argyi and Bioactive Metabolites From Diaporthe sp. AC1," *Front Microbiol*, vol. 13, Jun. 2022, doi: 10.3389/fmicb.2022.908836.
73. F. Tonial *et al.*, "Biological activity of Diaporthe terebinthifolii extracts against Phyllosticta citricarpa," *FEMS Microbiol Lett*, vol. 364, pp. 1–7, 2017, doi: 10.1093/femsle/fnx026.
74. X. Peng *et al.*, "New Xanthones with Antiagricultural Fungal Pathogen Activities from the Endophytic Fungus Diaporthe goulteri L17," *J Agric Food Chem*, vol. 69, no. 38, pp. 11216–11224, Sep. 2021, doi: 10.1021/acs.jafc.1c03513.
75. Y. Gao *et al.*, "Isolation and Characterization of Antifungal Metabolites from the Melia azedarach - Associated Fungus Diaporthe eucalyptorum," *J. Agric. Food Chem.*, vol. 68, no. 8, pp. 2418–2425, 2020, doi: 10.1021/acs.jafc.9b07825.

 doi:10.20944/preprints202512.0969.v1

76. D. C. Savi *et al.*, "Dihydroisocoumarins produced by Diaporthe cf . heveae LGMF1631 inhibiting citrus pathogens," *Folia Microbiol (Praha)*, vol. 65, pp. 381–392, 2020, doi: 10.1007/s12223-019-00746-8.
77. A. Stefan and A. Hochkoeppler, "The catalytic action of enzymes exposed to charged substrates outperforms the activity exerted on their neutral counterparts," *Biochem Biophys Res Commun*, vol. 751, p. 151436, Mar. 2025, doi: 10.1016/J.BBRC.2025.151436.
78. N. Borkakoti, A. J. M. Ribeiro, and J. M. Thornton, "A structural perspective on enzymes and their catalytic mechanisms," *Curr Opin Struct Biol*, vol. 92, p. 103040, Jun. 2025, doi: 10.1016/J.SBI.2025.103040.
79. H. C. Dorfmueller, A. T. Ferenbach, V. S. Borodkin, and D. M. F. Van Aalten, "A structural and biochemical model of processive chitin synthesis," *Journal of Biological Chemistry*, vol. 289, no. 33, pp. 23020–23028, Aug. 2014, doi: 10.1074/jbc.M114.563353.
80. M. Á. Curto, E. Butassi, J. C. Ribas, L. A. Svetaz, and J. C. G. Cortés, "Natural products targeting the synthesis of β(1,3)-D-glucan and chitin of the fungal cell wall. Existing drugs and recent findings," *Phytomedicine*, vol. 88, p. 153556, Jul. 2021, doi: 10.1016/J.PHYMED.2021.153556.
81. L. Belmonte and S. S. Mansy, "Patterns of Ligands Coordinated to Metallocofactors Extracted from the Protein Data Bank," *J Chem Inf Model*, vol. 57, no. 12, pp. 3162–3171, Dec. 2017, doi: 10.1021/ACS.JCIM.7B00468.